

# Equation of State and the Finite Temperature Transition in QCD

Rajan Gupta [HotQCD Collaboration]

Theoretical Division, Los Alamos National Laboratory, Los Alamos, NM 87545, USA

This talk provides a summary of the results obtained by the HotQCD collaboration on the equation of state and the crossover transition in 2+1 flavor QCD. We investigate bulk thermodynamic quantities - energy density, pressure, entropy density, and the speed of sound over the temperature range  $140 < T < 540$  MeV. These results have been obtained on lattices of temporal size  $N_\tau = 6$  and 8 and with two improved staggered fermion actions, asqtad and p4. Our most extensive results are with masses of the two degenerate light quarks set at  $m_l = 0.1m_s$  corresponding to the Goldstone pion mass  $m_\pi$  between  $220 - 260$  MeV. In these simulations, the strange quark mass is tuned to its physical value and constant values of  $m_l/m_s$  define lines of constant physics. We also summarize the current state of results on observables sensitive to the chiral and deconfining physics - the light and strange quark number susceptibilities, the chiral condensate and its susceptibility, and the renormalized Polyakov loop. Our results indicate that the deconfinement and chiral symmetry restoration occur in the same narrow temperature interval.

## 1. Introduction

Ongoing experiments at RHIC and proposed experiments at LHC aim to understand the properties of hot dense nuclear matter created in the collision of two relativistic nuclei. At sufficiently high temperatures and densities RHIC data support the creation of a quark-gluon plasma in the central region that undergoes a transition back to hadronic matter as it expands and cools. The goal is to explain the creation and evolution of this medium. Hydrodynamic descriptions used to model this evolution provide a good fit to the data and are thus the phenomenological tool of choice. First principle calculations using lattice QCD yield a number of properties of QCD as a function of temperature that are essential inputs in these hydrodynamical analyses. These properties include the nature of the transition (with respect to both confinement and chiral symmetry breaking) between the quark-gluon plasma and hadronic matter, the transition temperature, the equation of state of QCD and transport coefficients as a function of temperature in the range  $140 - 700$  MeV.

HotQCD is a US wide collaboration engaged in the study of QCD at finite temperature and density using lattice QCD<sup>1</sup>. It brought together members of the MILC and RBC-Bielefeld collaborations to carry out large scale simulations on IBM BlueGene/L supercomputers at the Lawrence Livermore National Lab and on the NYBlue at the New York Center for Computational Sciences at BNL.

Our goals are to perform detailed simulations of

2+1 flavor QCD using staggered fermions at the physical values of the strange and light quark masses. Most of the results presented here are for  $m_l = 0.1m_s$ , about a factor of two heavier than the mean physical  $u$  and  $d$  quark mass,  $m_l \approx 0.038m_s$ . Improvements in algorithms and computer resources are being used to incrementally approach the physical up and down quark masses and the continuum limit, thus providing high precision results. Also, in the current simulations the up and down quark masses are taken to be degenerate.

The physical quantities we are calculating include:

- The Equation of State (EoS) of QCD over the temperature range  $140 - 700$  MeV that is being probed by relativistic heavy ion experiments at Brookhaven and will be studied in more detail in the future at the LHC.
- The nature of the deconfinement transition between the hadronic phase at low temperature and the quark-gluon plasma at high temperatures. All simulations with staggered fermions show a rapid crossover rather than a genuine phase transition for physical values of the light quark masses. In the absence of a phase transition, there is *a priori* no unique transition temperature as it can depend on the probe. Thus, the temperature at which this transition takes place remains a subject of investigations. The status of current estimates is discussed at the end of this paper.
- The restoration of chiral symmetry at high temperature and whether this chiral transition is coincident with the deconfining transition.
- A detailed understanding of the physics in the transition region and the approach of thermodynamics quantities such as pressure, entropy, energy density and the speed of sound, to the Stefan-Boltzmann limit.

<sup>1</sup>HotQCD Collaboration members are: A. Bazavov, T. Bhattacharya, M. Cheng, N.H. Christ, C. DeTar, S. Ejiri, S. Gottlieb, R. Gupta, U.M. Heller, K. Huebner, C. Jung, F. Karsch, E. Laermann, L. Levkova, C. Miao, R.D. Mawhinney, P. Petreczky, C. Schmidt, R.A. Soltz, W. Soeldner, R. Sugar, D. Toussaint and P. Vranas

To understand and control systematic errors in the lattice calculations we are taking the following steps:

- Simulations at  $N_\tau = 4, 6,$  and  $8$  have been performed with two improved staggered fermion actions – asqtad and p4 – to understand  $O(a^2)$  discretization errors.
- Extrapolation to the continuum limit to remove discretization errors will be made using simulations at  $N_\tau = 6, 8$  and a new set of  $N_\tau = 12$  lattices.
- The theory possesses a chiral phase transition in the limit  $m_l = 0$ . To study the chiral behavior, extrapolations to the physical light quark mass limit and the chiral limit will be made using simulations at  $m_l/m_s = 0.2, 0.1$  and  $0.05$ .
- The transition region,  $160 - 230$  MeV, is being sampled in intervals of  $5$  MeV or less using high statistics simulations in order to pin down the position of the peak in the chiral susceptibility and the inflection point in the light quark number susceptibility.

The first part of this report summarizes results for the equation of state obtained by the HotQCD collaboration [1]. In the second part we discuss our results for the temperature dependence of the chiral and deconfining transitions and finally compare these results against recent data presented by the Wuppertal-Budapest collaboration [2].

## 2. Setup of Lattice Calculations

To determine the lattice parameters for a systematic finite temperature analysis, zero temperature simulations are used to first set the lattice scale  $a$  and the physical value of the strange quark mass as a function of  $\beta$ . The scale  $a$  is extracted using the Sommer scale  $r_0$  obtained from the derivative of the static  $q\bar{q}$  potential evaluated on the lattice

$$\left( r^2 \frac{dV_{q\bar{q}}}{dr} \right)_{r=r_0} = 1.65 \quad (1)$$

with  $r_0 = 0.469(7)$  fm taken from the Upsilon  $2S - 1S$  splitting [3]. The strange quark mass is then set using the  $s\bar{s}$  pseudoscalar meson state with  $M_{s\bar{s}}r_0 = 1.58$ .

The last quantity to fix are the light (up and down) quark masses that are taken to be degenerate. We define lines of constant physics (LCP) by keeping  $m_l/m_s$  fixed. In our calculations three values of  $m_l/m_s = 0.2, 0.1$  and  $0.05$  are being simulated. Results for the physical value of the light quark mass are then obtained by extrapolation in  $m_l$  at fixed lattice scale. With these definitions, the continuum limit along a

LCP can be taken by varying a single parameter, the gauge coupling  $\beta \rightarrow \infty$  or equivalently  $a \rightarrow 0$  since  $\beta$  and  $a$  are related by dimensional transmutation in QCD. The results presented here are obtained mostly for  $m_l/m_s = 0.1$  with  $N_\tau = 6$  and  $8$  lattices, so estimates of extrapolated values and uncertainties in them should be considered preliminary.

In the finite temperature calculations, the temperature  $T$ , lattice scale  $a$  and the size of the lattice in the temporal direction  $N_\tau$  are related as  $T = 1/aN_\tau$ . For fixed  $N_\tau$  we increase  $T$  by decreasing  $a$  or equivalently increasing  $\beta$ , and adjusting  $m_s$  for each  $\beta$ .

There are two overarching issues with the use of staggered fermions. Both have to do with the fact that staggered fermions preserve a residual chiral symmetry at the expense of a 4-fold doubling of flavors, i.e., every continuum quark flavor develops four copies on the lattice. These four copies are called taste. The first issue with using staggered quarks is one of principal. To simulate a single flavor (say an s quark) we take the fourth root of the fermion determinant in calculating the fermion force in Monte Carlo simulations. Creutz [4] has argued that a strong mixing of tastes with different chiralities leads to an incorrect 't Hooft vertex, and concludes that rooting can often be a good approximation but predictions for non-perturbative physics where the 't Hooft vertex is important can not be trusted. On the other hand Sharpe [5] and Goltermann [6] argue that while this rooting trick is ugly a well defined continuum limit exists and the theory recovered in this limit is QCD. Numerical results obtained with staggered fermions when compared to experimental data indicate that the rooting trick works [7] *i.e.* this circumstantial evidence provide support that staggered simulations reproduce QCD. Clearly, our calculations rely on the validity of the arguments reviewed by Sharpe and Golterman. In short, our work does not shed any independent light on this issue.

The second issue is that, at finite lattice spacings, the 4 copies called tastes, are not degenerate and the taste symmetry is badly broken for both asqtad and p4 actions at  $1/a \leq 2$  GeV corresponding to the transition region for  $N_\tau \leq 8$  simulations. This issue is being explored and improved versions of the staggered action are being designed to reduce this breaking. The most severe impact of this breaking is in the pion sector. In our p4 action calculations with  $m_l/m_s = 0.1$  on  $N_\tau = 8$  lattices, the mass of the Goldstone pion is  $M_{\pi 0} r_0 \approx 0.52$  corresponding to  $M_\pi \approx 220$  MeV while the other fifteen higher mass taste flavor pions are at 440 MeV or heavier. The splitting for asqtad action is slightly smaller. We expect this violation of taste symmetry to affect the results in the low temperature confined phase and in the transition region where the dominant excitations are pions. Unfortunately, at this point we do not have a good estimate of the uncertainty introduced in the various quantities

we calculate due to taste symmetry breaking.

The single basic quantity given by lattice simulations en-route to calculating thermodynamics variables such as the pressure and energy density is the trace anomaly  $\Theta^{\mu\mu}a^4 = (\varepsilon - 3p)a^4$ . We first discuss the data for it and the extraction of the EoS from it. The second part introduces probes used to understand the nature and location of the deconfining and chiral symmetry restoration transitions and presents our data. Finally we compare these results to those from the Wuppertal-Budapest collaboration [2].

### 3. Trace Anomaly $(\varepsilon - 3p)/T^4$

The calculation of  $\Theta^{\mu\mu}a^4$  involves calculating terms that make up the gauge and fermion actions. As a result, most of the computer time is spent in generating the ensemble of statistically independent gauge configurations. Results presented here represent over 100 million node hours on the BlueGene/L.

Data for  $(\varepsilon - 3p)a^4$  is converted into physical units using the scale  $r_0$  and subsequently in units of the temperature  $T$  as shown in Fig. 1. Overall, the data show that the asqtad and p4 actions give consistent results, with differences consistent with the expected magnitude of  $O(a^2)$  errors. The details are highlighted in figures 2, 3, 4 and discussed below.

From the trace anomaly the pressure is obtained using the relations

$$\begin{aligned} \frac{\Theta^{\mu\mu}}{T^4} &\equiv \frac{\varepsilon - 3p}{T^4} = T \frac{\partial}{\partial T} \left( \frac{p}{T^4} \right) \\ \frac{p(T)}{T^4} - \frac{p(T_0)}{T_0^4} &= \int_{T_0}^T dt \frac{\Theta^{\mu\mu}(t)}{t^5} \end{aligned} \quad (2)$$

The energy density, entropy density  $(\varepsilon+p)/T^4$  and the speed of sound are then given by appropriate combinations of  $(\varepsilon - 3p)/T^4$  and  $p/T^4$ .

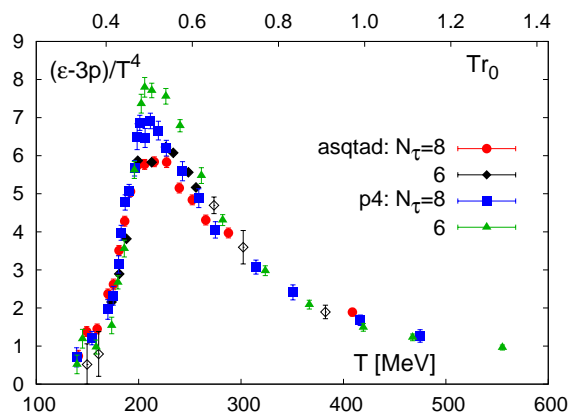


Figure 1: Data for the trace anomaly  $(\varepsilon - 3p)/T^4$  calculated using the asqtad and p4 actions at  $N_\tau = 6, 8$ . This is the single basic quantity obtained from lattice simulations.

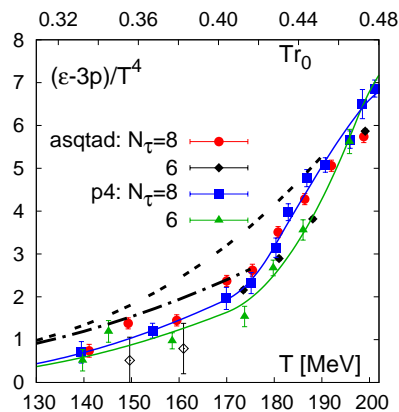


Figure 2: Details of  $(\varepsilon - 3p)/T^4$  in the range 140 – 200 MeV.

**Low Temperature Region:** Comparing  $N_\tau = 6$  and 8 data in Fig. 2 for the low temperature region show a  $\sim 5$  MeV shift towards lower temperatures under  $N_\tau = 6 \rightarrow 8$ . This shift is indicative of  $O(a^2)$  discretization errors. To calculate the pressure using Eq. 2 we need to fit the data obtained at a discrete set of points to a functional form that can be integrated and fix the normalization of  $\Theta^{\mu\mu}$  at some low starting temperature  $T_0$ . We first discuss the normalization and return to the determination of the functional form in the next section. For  $T < 150$  MeV, the discretization errors in lattice simulations, especially those due to the large taste symmetry violations in asqtad and p4 staggered actions, are pronounced so  $N_\tau = 8$  data have unknown systematic uncertainties. We, therefore, explore predictions of the hadron resonance gas (HRG) model as it is an independent method in which control over systematic uncertainties improves as  $T$  is taken below the pion mass scale  $M_\pi = 140$  MeV [8]. In Fig. 2 we plot results for two choices of the cutoff scale  $m_{max}$  up to which resonances are included,  $m_{max} = 1.5$  GeV (dot dashed black curve) and 2.5 GeV (upper dashed curve). Unfortunately, the HRG estimates show significant sensitivity to the cutoff  $m_{max}$  for  $T > 100$  MeV. Also, there is no matching point  $T_0$  between lattice and the HRG data. There is a trend in the lattice results to move towards the HRG values as  $a \rightarrow 0$ , i.e., as  $N_\tau = 6 \rightarrow 8$ , however, at this point, we do not have a way to quantify it, and conclude that further work is required to reduce the uncertainty associated with the choice of normalization.

**Intermediate (Peak) Region:** Figure 3 shows that the peak in  $\Theta^{\mu\mu}/T^4$  occurs at  $T > 200$  MeV. The differences between the asqtad and p4 results for  $N_\tau = 6$  versus 8 are the largest in the interval  $200 \leq T \leq 300$  and show a 15 – 20% effect at the peak. We also find that the peak in the asqtad data is shallower and shows smaller difference between  $N_\tau = 6$  and 8

values as compared to the p4 results.

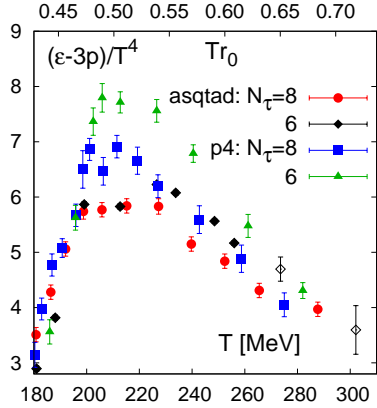


Figure 3: Details of  $(\varepsilon - 3p)/T^4$  over the range 180 – 300 MeV.

**High temperature region  $T > 300$  MeV:** Data in Fig. 4 show that the two actions give consistent results and the difference between  $N_\tau = 6$  and 8 are small.  $\Theta^{\mu\mu}/T^4$  should, at sufficiently high temperatures, vanish as  $g^4(T)$ , however, between 300 – 700 MeV the data show a much faster variation. We, therefore, use the ansatz

$$\frac{\varepsilon - 3p}{T^4} = \frac{3}{4}b_0g^4 + \frac{d_2}{T^2} + \frac{d_4}{T^4} \quad (3)$$

to fit the data. Fits show no sensitivity to the leading  $g^4$  term. Consequently, this term is neglected in the fits shown in Fig. 4 and used for the extraction of  $p$ .

To improve these fits and determine the shape of the curves for  $T > 300$  MeV two enhancements to our data sets are needed. First, we need data at more points. Second, checks for finite volume corrections need to be made for  $T > 500$  MeV when the lattice size in the spatial directions used in the simulations,  $N_s = 32$ , approaches  $N_s a = 1/160$  for  $a$  in  $\text{MeV}^{-1}$ . Here  $a$  corresponds to the zero temperature scale at each of the the gauge couplings used to simulate  $T > 500$  MeV lattices, and the temperature scale 160 MeV is used as it marks the rapid onset of thermal fluctuations as shown in Fig 1.

### 3.1. Fits to $\Theta^{\mu\mu}/T^4$ and extraction of $p$

To extract the behavior of  $p$  versus  $T$  using Eq. 2 we need to fit the data for  $\Theta^{\mu\mu}/T^4$  calculated at a discrete set of points with a smooth function. We do this using a piecewise smooth interpolation. For  $T < 170$  MeV an exponential fit is used, while for  $170 < T < 250$  MeV separate quadratic fits over several intervals were used. We found it necessary to match the function and its derivative at each end of these intervals to get a smooth curve for  $p$ . For  $T > 250$  MeV the result of the fit with the form given in Eq. 3 is used. These fits

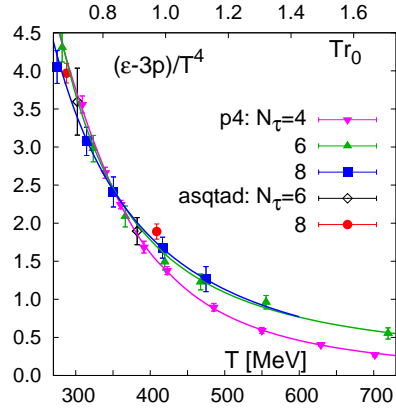


Figure 4: Details of  $(\varepsilon - 3p)/T^4$  over the range 300 – 700 MeV.

are shown for both actions and for  $N_\tau = 6$  and 8 in Figures 5.

The fits are very similar in shape for the two actions. In each case shifting the fits to  $N_\tau = 6$  data by  $\approx 5$  MeV to lower temperatures give much better agreement except for the height of the peak in the p4 data. This shift by 5 MeV suggests the size of discretization errors coming from a combination of (i) the errors in the finite  $T$  simulations and (ii) from the scale  $a$  extracted from zero temperature simulations clustered around  $\beta$  values corresponding to the two peak regions for  $N_\tau = 6$  and 8.

Our results for  $p$  using Eq. 2 (and consequently all other thermodynamic quantities) are obtained with the normalization  $p = 0$  at  $T = T_0 = 0$  and requiring the fit to the lattice data to pass through this point. Redoing the fits starting with the HRG value at  $T = 100$  MeV results in a global shift in the pressure and energy density curves by  $\approx 0.8$ . The size of this effect is illustrated by the black square at  $T = 550$  MeV in Fig. 6.

Once  $(\varepsilon - 3p)/T^4$  and  $p/T^4$  are known we get the other thermodynamics quantities; entropy density as  $(\varepsilon + p)/T^4$  and the speed of sound by using the ratio  $p/\varepsilon$  in

$$c_s^2 = \frac{dp}{d\varepsilon} = \varepsilon \frac{d(p/\varepsilon)}{d\varepsilon} + \frac{p}{\varepsilon}. \quad (4)$$

These results are shown in Figures 7 and 8. We regard the spread in the results between the two actions as indicative of discretization errors.

In Figures 6 and 7 we highlight the band 185 – 195 MeV which we estimate covers the inflection point in the energy density  $\varepsilon$  and the entropy density data. Both of these thermodynamics quantities probe deconfinement – the change in the thermodynamics as the degrees of freedom evolve from hadrons to quarks and gluons due to the change in their free energies. Note that while we discuss other probes of deconfinement and chiral symmetry restoration later, it is

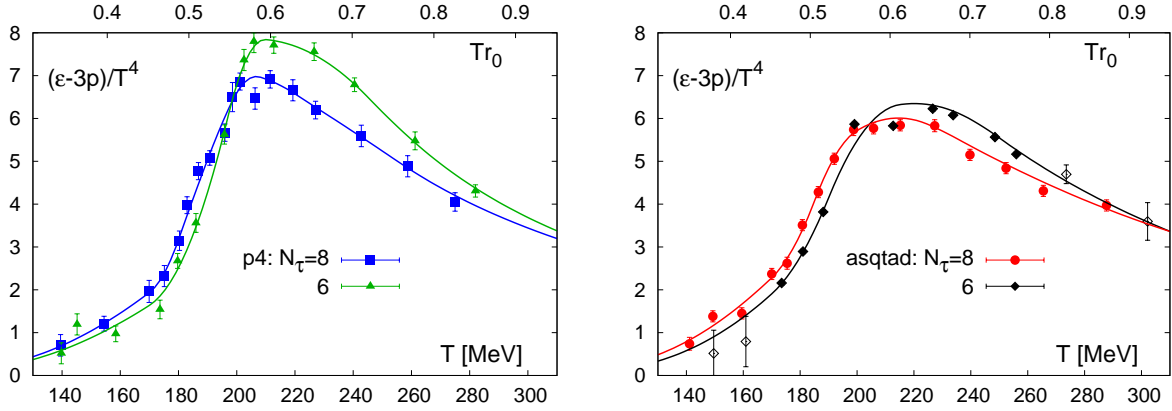


Figure 5: Fits to  $\Theta^{\mu\mu}/T^4$  data for the p4 lattice action (left panel) and the asqtad action (right panel).

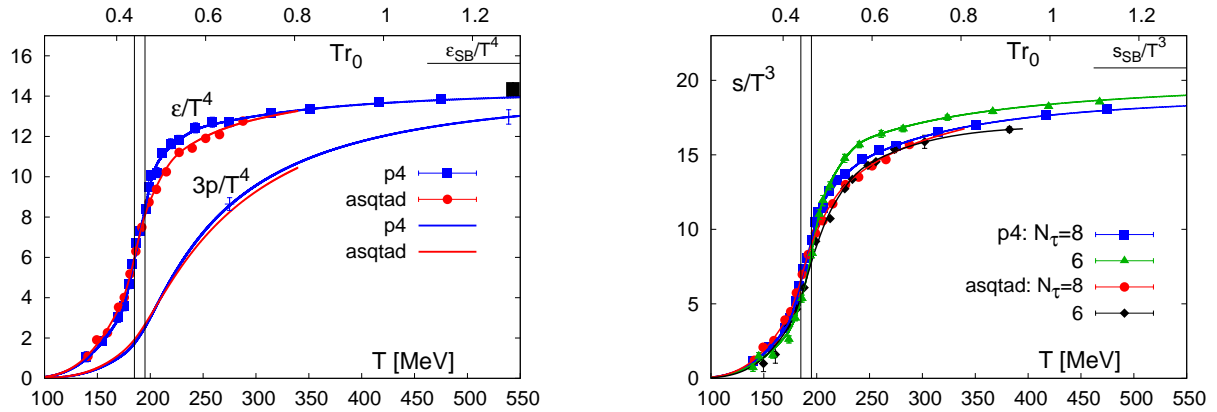


Figure 6: Results for the energy density  $\epsilon/T^4$  and the pressure  $3p/T^4$  for the two actions obtained on  $N_\tau = 8$  lattice with  $m/m_s = 0.1$ .

these thermodynamic quantities that are inputs in the hydrodynamic analysis of RHIC data.

Our data show that for  $T > 300$  MeV the degrees of freedom are quarks and gluons and the deviations from the Stefan-Boltzmann limit are 10 – 15%. Thus experiments at the LHC, which will probe the full range  $140 < T < 700$  MeV, will be able to explore the behavior and nature of collective excitations in the quark-gluon plasma. Even though the HotQCD estimates for the EoS do not include extrapolation to the continuum limit and physical light quark masses, we propose that they are realistic and ready for use in phenomenological analyses.

#### 4. The Deconfining and Chiral Transition

The data presented in previous sections show that the transition from hadronic matter to quark-gluon plasma is a rapid crossover and not a genuine phase

Figure 7: The entropy density obtained on lattices with temporal extent  $N_\tau = 6$  [9, 10] and 8.

transition. This is consistent with all existing calculations with staggered fermions. We expect a singularity in the partition function to exist in the chiral limit. What remains to be settled for QCD with a physical value of the strange quark mass is whether this phase transition occurs only at zero light quark masses ( $m_l \equiv m_{crit} = 0$ ) or at small but nonzero value ( $m_l \equiv m_{crit} > 0$ ). In the first case the transition would belong to the universality class of the 3-dimensional  $O(4)$  symmetric spin model and in the latter case to the 3 – d Ising model [11].

In light of this expected behavior, the questions that we would like to answer regarding the nature and location of the transition from hadronic matter to quark-gluon plasma in QCD are:

- How is the observed crossover in thermodynamic quantities for physical light and strange quark masses influenced by the chiral phase transition?
- What do standard probes of deconfinement (expectation value of Polyakov loop and quark number susceptibilities) and chiral symmetry

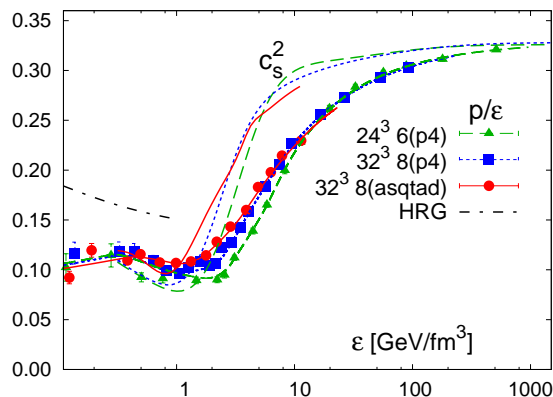


Figure 8: Data for  $p/\epsilon$  and the speed of sound extracted from it. Lines without data points are obtained using the interpolating functions shown in Figures 5. The dash-dot line is the HRG estimate.

restoration (chiral condensate and the chiral susceptibility) tell us?

- Do the crossovers indicating deconfinement and chiral symmetry restoration happen at the same temperature (we will denote these as  $T_c$  but note that it represents the crossover temperature and not a critical temperature) and what are the mechanisms that drive them?

Our results for the various probes are presented next.

#### 4.1. Renormalized Polyakov Loop

The logarithm of the expectation value of the Polyakov loop is related to the free energy of an isolated quark,

$$\langle L \rangle \sim \exp(-F_q/T). \quad (5)$$

In QCD  $\langle L \rangle$  is not a genuine order parameter, *i.e.*, zero in the confined phase and non-zero in the deconfined phase, for any finite values of the quark masses. As far as we know, the Polyakov loop is not directly sensitive to the singular structure of the partition function in the chiral limit. It does, however, exhibit a broad crossover as shown in Fig. 9 where we plot the renormalized quantity  $\langle L_{ren} \rangle = Z(\beta)^{N_\tau} \langle L \rangle$  [10]. The renormalization is needed to remove the self-energy contributions to the free energy.

Data for  $\langle L_{ren} \rangle$  exhibit a gradual rise rather than a rapid crossover. This feature is also reflected in the lack of a peak in its susceptibility. We find only a broad shoulder after the rise for all data with  $N_\tau \geq 6$  lattices. Since there is no well defined inflection point in  $\langle L_{ren} \rangle$  or a peak in its susceptibility we do not consider it a reliable probe and argue it should not be used in precision studies to determine the location of a crossover  $T_c$  indicative of deconfinement.

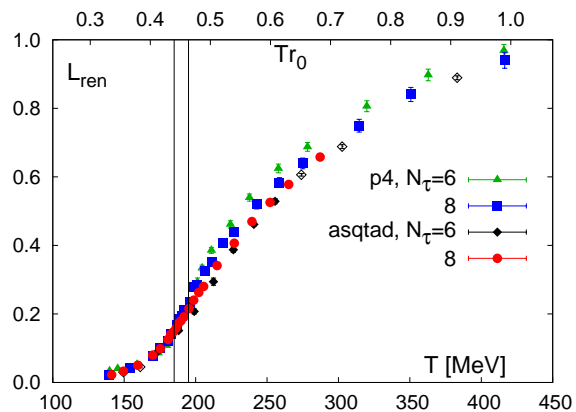


Figure 9: Data for the Polyakov Loop  $\langle L_{ren} \rangle$ . Note the gradual rise in contrast to the rapid crossover seen in thermodynamic quantities.

#### 4.2. Quark Number Susceptibility

Thermal fluctuations of the degrees of freedom that carry a net number of light or strange quarks are probed by taking derivatives of the partition function with respect to the corresponding chemical potential,

$$\frac{\chi_q}{T^2} = \frac{1}{VT^3} \left( \frac{\partial^2 \ln Z}{\partial(\mu_q/T)^2} \right)_{\mu_q=0}, \quad q = l, s. \quad (6)$$

The quark number operator  $\bar{\psi}\gamma_0\psi$  is a good probe in lattice calculations since it does not require normalization. It counts the charge  $N_q$ , *i.e.*, the net number of light or strange quarks. Similarly  $\chi_q \sim \langle N_q^2 \rangle$ . Therefore, in the continuum and infinite temperature limit  $\lim_{T \rightarrow \infty} \chi_q/T^2 = 1$ , the Stefan-Boltzmann value for an ideal massless one flavor quark gas. The approach to unity in our data for the light quarks is shown in Fig. 10.

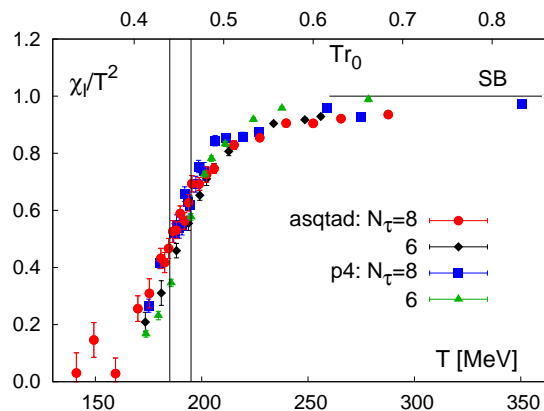


Figure 10: Data for the light quark number susceptibility  $\chi_l/T^2$ . Note the crossover is consistent with the band at 185 – 195 MeV and the value approaches unity rapidly after 250 MeV.

As the transition region is approached from above, hadronic states with appropriate quantum numbers start to contribute in proportion to their Boltzmann weight  $\sim \exp(-M/T)$ . At low temperatures the dominant contributions are from the lightest hadronic state that has the correct quantum numbers, *i.e.*,  $\chi_s/T^2 \sim \exp(-M_K/T)$ , while  $\chi_l/T^2 \sim \exp(-M_\pi/T)$ . Since  $M_K$  remains finite in the limit  $m_l \rightarrow 0$ , only  $\chi_l/T^2$  is directly sensitive to singularities in the QCD partition function in the chiral limit. This expectation is confirmed by comparing the behavior of  $\varepsilon/\chi_s T^2$  versus  $\varepsilon/\chi_l T^2$  in Fig. 11. Below the transition region  $\varepsilon/\chi_s T^2$  rises rapidly in contrast to  $\varepsilon/\chi_l T^2$ . In fact it will diverge because  $\chi_s$  is not sensitive to the lightest hadrons and goes to zero faster than  $\varepsilon$  which does receive contributions from the pions. We therefore claim that  $\chi_l/T^2$  and not  $\chi_s/T^2$  should be used to probe the singular structure of the theory.

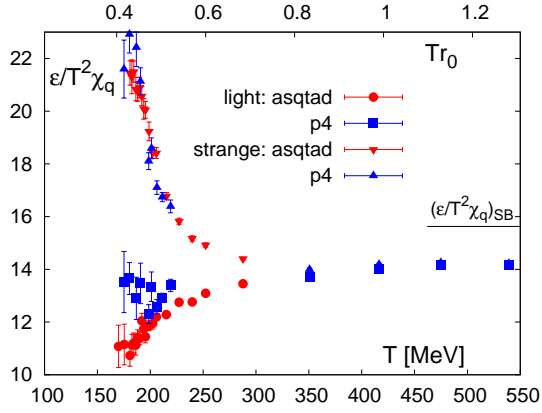


Figure 11: Comparison of the strange and light quark number susceptibility in units of the energy density, *i.e.*  $\varepsilon/\chi_s T^2$  versus  $\varepsilon/\chi_l T^2$ .  $\varepsilon/\chi_s T^2$  is seen to grow rapidly and is expected to diverge as  $m_l \rightarrow 0$  since  $\varepsilon$  gets contributions from the pions while  $\chi_s \rightarrow 0$  as  $\exp(-M_K/T)$ .

The data for  $\chi_l/T^2$  in the transition region (see Fig. 10) show a rapid crossover with the location of the inflection point again consistent with the band 185 – 195 MeV. We therefore conclude that all probes of the deconfinement transition,  $\varepsilon$ , the entropy density and  $\chi_l/T^2$ , give consistent results.

### 4.3. Chiral Condensate and Susceptibility

The light and strange quark chiral condensates are given by the derivatives of the free energy with respect to the quark masses:

$$\langle \bar{\psi}\psi \rangle_q = \frac{T}{V} \frac{\partial \ln Z}{\partial m_q}, \quad q = l, s, \quad (7)$$

At finite values of the quark masses  $\langle \bar{\psi}\psi \rangle_q$  requires both multiplicative and additive renormalizations.

Both renormalizations are performed by defining the following subtracted quantity for light quarks

$$\Delta_{l,s}(T) = \frac{\langle \bar{\psi}\psi \rangle_{l,T} - \frac{m_l}{m_s} \langle \bar{\psi}\psi \rangle_{s,T}}{\langle \bar{\psi}\psi \rangle_{l,0} - \frac{m_l}{m_s} \langle \bar{\psi}\psi \rangle_{s,0}}. \quad (8)$$

The subtractions proportional to  $\langle \bar{\psi}\psi \rangle_s$  remove the singular part of the additive renormalization proportional to  $m_q/a^2$ . Division by the  $T = 0$  estimate obtained at the same lattice scale  $a$  cancels the multiplicative renormalization as it is  $T$  independent.

Data for  $\Delta_{l,s}(T)$  along the LCP given by  $m_l = 0.1m_s$  are shown in Fig. 12. We find a rapid crossover in the same temperature range as exhibited by the bulk thermodynamic observables and the light quark number susceptibility. This indicates that deconfinement and chiral symmetry restoration happen at the same temperature.

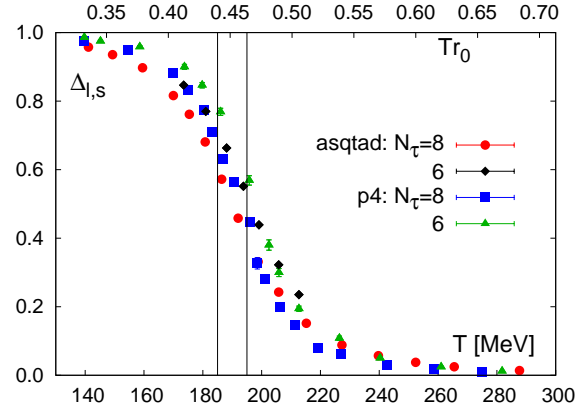


Figure 12: p4 and asqtad data for the renormalized chiral condensate  $\Delta_{l,s}(T)$  along the LCP given by  $m_l = 0.1m_s$ .

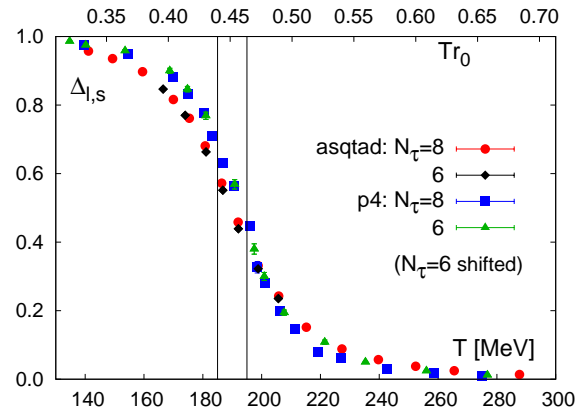


Figure 13: Same data as in Fig. 12 for the renormalized chiral condensate  $\Delta_{l,s}(T)$  but with the  $N_\tau = 6$  data shifted to the left by 5 MeV for each action.

To estimate the magnitude of the difference between  $N_\tau = 6$  and 8 data we plot, in Fig. 13, the same data

after shifting the  $N_\tau = 6$  values by 5 MeV to the left. The results for  $N_\tau = 6$  and 8 lattices now come together. The replot also brings out the difference in results between the two actions — the difference is in the shape of curves. The data with the p4 action shows a slightly steeper crossover. Based on Fig. 13 we estimate that both systematic effects are  $\sim 5$  MeV and the location of the inflection point is covered by the band 185 – 195 MeV shown by the vertical lines.

The chiral susceptibility is given by the second derivative of  $\ln Z$  with respect to the quark mass  $m$ :

$$\begin{aligned} \frac{\chi_{l,s}}{T^2} &= \frac{T}{V} \left( \frac{\partial^2 \ln Z}{\partial^2 (m_{l,s}/T)^2} \right) \\ &= \langle \text{Tr}(M_{l,s}^{-2}) \rangle \\ &\quad + \frac{1}{4} \left( \langle (\text{Tr} M_{l,s}^{-1})^2 \rangle - \langle \text{Tr} M_{l,s}^{-1} \rangle^2 \right), \quad (9) \end{aligned}$$

where the first term in the right hand side gives the contributions of connected Feynman diagrams and the second gives those from the disconnected diagrams.  $\chi_l$  is the best probe of the chiral transition as it exhibits a peak even when the theory has a crossover and it will diverge at the chiral phase transition, *i.e.*, in the chiral limit. The location of the peak is used to mark  $T_c$ .

Preliminary unpublished data from the  $N_\tau = 8$  simulations is shown in Fig. 14. The left hand figure shows data for  $m_l/m_s = 0.2, 0.1$  and  $0.05$  for the two actions. We find that the height of the peak grows with decreasing quark mass and is expected to diverge with an exponent  $1/\delta - 1$  corresponding to the  $O(4)$  universality class of the chiral transition.

The second noteworthy feature is that the peak is broad and its width increases with decreasing quark mass. This is also expected because in the chiral limit the pions are massless for all values of  $T \leq T_c$  and give rise to a singularity in the “magnetic” part of the free energy, and the chiral susceptibility is expected to diverge as  $m_l^{1/2}$  [12]. The plot on the right hand side shows the same data scaled by  $(m_l/m_s)^{1/2}$ . The peaks in the three data sets collapse together, consistent with the expected  $m_l^{1/2}$  behavior. We do not find simultaneous evidence for the expected  $O(N)$  scaling of the height of the peak mentioned above. This dual scaling behavior raises the question – what point should be labeled as  $T_c$ ? In the absence of a clear peak, we will choose the right edge to denote the chiral symmetry restoration temperature  $T_c^{\text{chiral}}$ .

The third feature shown by the data is that the location of the peak moves to lower temperatures with decreasing quark mass. For  $m_l = 0.1m_s$  the location is consistent with the 185–195 MeV range found earlier, however, the trend suggests a lower value (by 5 – 10 MeV) in the physical quark mass limit [13]. Similarly, the location of the peak in the asqtad action is shifted with respect to p4 to lower temperatures at each value of the quark mass by  $\sim 5$  MeV.

The bottom line is that we have identified a number of systematic uncertainties that are each  $\sim 5$  MeV and go in the same direction of lowering the estimate for  $T_c$ . It is therefore necessary that the continuum along  $m_l = 0.038$  LCP is taken in order to extract physical results.

## 5. Continuum Limit and HotQCD Plans for the Future

The results presented in the previous sections have been obtained on lattices with  $N_\tau = 6$  and 8 along a LCP defined by  $m_l = 0.1m_s$ . Two extrapolations are needed to obtain physical results. These are extrapolations in the light quark mass to the physical value  $m_l \approx 0.038$  and the continuum limit  $N_\tau \rightarrow \infty$  with  $a \rightarrow 0$ . The present data do not allow us to make either extrapolation reliably.

A number of simulations are in progress to address these two limitations:

- For both asqtad and p4 actions and for  $N_\tau = 6$  and 8 lattices we are completing simulations at three values of the light quark masses, *i.e.*  $m_l/m_s = 0.2, 0.1$  and  $0.05$ . These data will allow us to make extrapolations to the physical quark mass and the chiral limit.
- Having established in this study that asqtad and p4 actions give consistent results, we have started new asqtad simulations with  $N_\tau = 12$  and  $m_l = 0.05m_s$ . The combined data at  $N_\tau = 6, 8$  and 12 will allow us to take the continuum limit along the LCP defined by  $m_l = 0.05m_s$  and extrapolated data at  $m_l = 0.038m_s$ .
- We are exploring the Highly Improved Staggered Quark (HISQ) action [14] which has been designed to improve both the  $O(a^2)$  scaling behavior and reduce taste symmetry violations [15]. As mentioned earlier, the uncertainties associated with taste symmetry violations are not well understood and could be large.

## 6. Comparison of $T_c$ with Results from the Wuppertal-Budapest Collaboration

The Wuppertal-Budapest collaboration (WBC) has recently presented the following results on the location of the crossover indicating deconfinement and chiral symmetry restoration:

$$\begin{aligned} T_c &= 146(2)(3) \text{ MeV} \quad \text{Chiral,} \\ T_c &= 170(4) \text{ MeV} \quad \text{Deconf.} \quad (10) \end{aligned}$$

WBC results include extrapolation to the continuum limit using  $N_\tau = 8, 10, 12$  lattices along the  $m_l =$

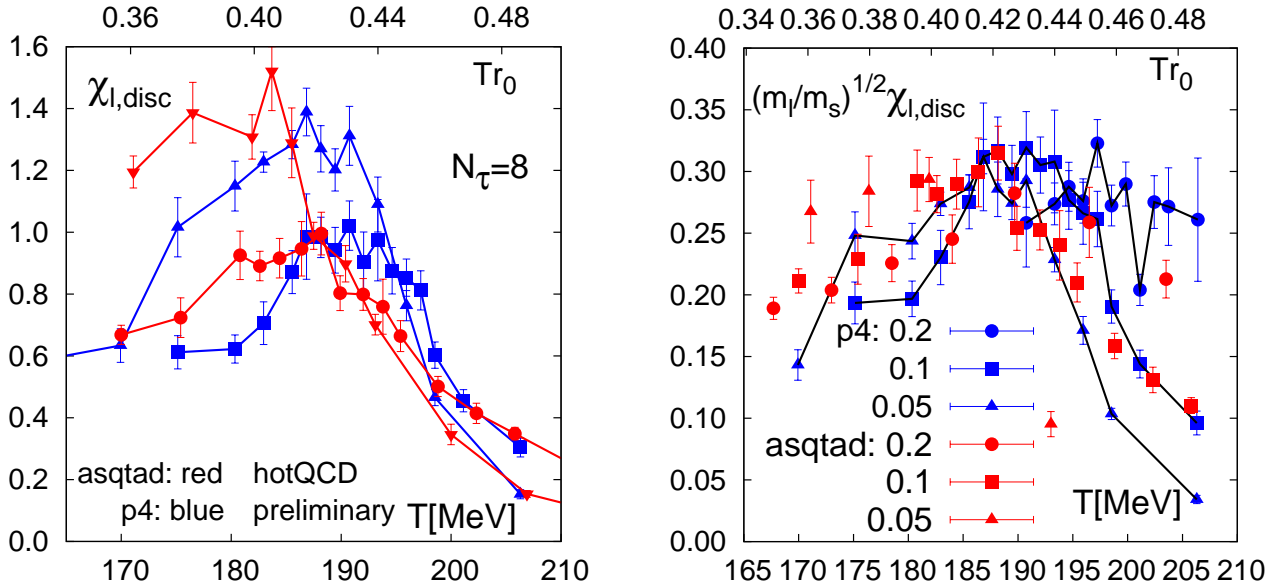


Figure 14: Preliminary HotQCD data for the disconnected part of the chiral susceptibility  $\chi_l(T)$  for the p4 and asqtad actions with  $N_\tau = 8$  and three values of the quark mass  $m_l/m_s = 0.2, 0.1$  and  $0.05$ . The right panel shows the same data as in the left panel but scaled by  $(m_l/m_s)^{1/2}$ . The behavior of the peak as a function of the quark mass is discussed in the text for both panels.

$0.04m_s$  LCP and are therefore labelled “physical”. They raise the following two issues when comparing to the HotQCD results discussed earlier.

- The WBC estimate for the chiral transition at 146(2)(3) MeV is about 40 MeV lower than the HotQCD results.
- The crossover in the chiral symmetry and deconfinement sectors are distinct and separated by  $\approx 24$  MeV whereas all HotQCD data indicate they are coincident.

Of these, we consider the difference in the location of the chiral transition the more significant issue that needs to be resolved. The reasons for discounting the difference in the location of  $T_c^{\text{deconf}}$  as significant are

- The best HotQCD data are on  $N_\tau = 8$  with  $m_l = 0.1m_s$  lattices. Three systematic effects, each shifting the estimate by  $\approx 5$  MeV to lower temperatures, have been identified. These are (i) the difference between  $N_\tau = 6$  and 8 lattice data; (ii) extrapolation in light quark masses and (iii) the difference between asqtad and p4 data. A fourth possible shift of 5 MeV arises from the recent change in the experimental value of  $f_K$  which resulted in lowering the WBC results by  $\sim 5$  MeV [2]. This change affects the continuum extrapolation carried out by the WBC and not the HotQCD results presented at fixed  $a$  with the scale set by  $r_0$ . All four factors are not necessarily independent, however, the point we want to make is that the difference

between 170(4) and 185 – 195 MeV can largely be accounted for by a combination of these systematic effects.

- More important, we have presented reasons for why the two methods used by the WBC to extract  $T_c^{\text{deconf}}$ , the Polyakov loop and strange quark number susceptibility, do not probe the singular structure of the theory. Our contention is that all previous results based on these probes do not qualify as precision measurements.
- Probes sensitive to the singular structure (energy and entropy density and the light quark number susceptibility) show the two transitions to be coincident for all values of the lattice parameters simulated by the HotQCD collaboration. It remains to be seen if this conclusion survives after extrapolation to the continuum limit.

The difference in  $T_c^{\text{chiral}}$  is less significant than it appears. All three systematic effects in HotQCD calculations discussed above as well as the change in WBC estimates on using the new experimental value of  $f_K$  are again applicable. Even though the WBC find that the five quantities ( $r_0$ , the new experimental value of  $f_K$ ,  $M_\Omega$ ,  $M_{K^*}$  and  $M_\phi$ ) used to set the lattice scale give consistent estimates in the continuum limit, there can be systematic differences when working at a given  $a$  as is the case for the HotQCD data. Assuming these four  $\sim 5$  MeV shifts add, as data indicate, the HotQCD estimate would be lowered to  $\sim 170$  MeV in the continuum. This, however, still leaves a difference of about 24 MeV that needs to be resolved.

The good news is that the HotQCD simulations underway will allow us to extrapolate to the continuum limit and to the physical light quark mass and thus shed light on these issues. We hope to have these results within the next year.

## Acknowledgments

I thank Derek Teaney for inviting me to present the HotQCD results at this meeting and to participate in exciting discussions on the RHIC program.

## References

- [1] A. Bazavov, *et al.* *Phy. Rev.* **D80**, 014504 (2009).
- [2] Y. Aoki, *et al.* *JHEP* 0906:088, 2009.
- [3] M. Wingate *et al.* *Phy. Rev. Lett.* **92** 162001 (2004).
- [4] M. Creutz, PoS **LAT2007**, 007 (2007).
- [5] S. R. Sharpe, PoS **LAT2006**, 022 (2006).
- [6] M. Golterman, PoS **CONFINEMENT8**, 014 (2008).
- [7] S. Durr, PoS **LAT2006**, 021 (2005).
- [8] A. Andronic *et al.* *Nucl. Phys.* **A722**, 167 (2006).
- [9] C. Bernard *et al.*, *Phys. Rev. D* **75**, 094505 (2007).
- [10] M. Cheng *et al.*, *Phys. Rev. D* **77**, 014511 (2008).
- [11] C. Bernard *et al.* [MILC Collaboration], *Phys. Rev. D* **71**, 034504 (2005).
- [12] F. Karsch, *Nucl. Phys.* **A820**, 99c (2009).
- [13] M. Cheng *et al.*, arXiv:0911.2215 [hep-lat].
- [14] E. Follana *et al.* *Phy. Rev* **D75**, 054502 (2007).
- [15] A. Bazavov and P. Petreczky [HotQCD Collaboration], PoS LAT2009, 163 (2009)